Simulation and analysis of the pneumatic recovery for side-cutting loss of combine harvesters with CFD-DEM coupling approach

Tao Jiang[1], Min Zhang[1], Zhuohuai Guan[1,2*], Senlin Mu[1], Chongyou Wu[1], Gang Wang[1], Haitong Li[1],

(1. *Nanjing Institute of Agricultural Mechanization, Ministry of Agriculture and Rural Affairs, Nanjing 210014, China*;
2. *Synergistic Innovation Center of Jiangsu Modern Agricultural Equipment and Technology, Zhenjiang 212013, Jiangsu, China*)

Abstract: A novel pneumatic recovery method was proposed to curb the problem of high losses caused by side-cutting in a rapeseed combine harvester header. The influence of recovery method and material status changes on the recovery effect was studied via the CFD-DEM (computational fluid dynamic- discrete element method) coupling simulation. The effect of airflow action on the recovery effect was compared and analyzed, and the composite pneumatic recovery method was determined. In addition, the influence of material status changes and material feeding rate on the recovery effect was explored, and the critical condition of material blockage in the recovery device was configured. As such, the relationship model between air velocity and recovery rate was constructed and the air distribution ratio of the flow field in the device under this condition was optimized, had verified the rationality of this pneumatic recovery method was verified by a series of field tests. The average rapeseed recovery rate of 92.95% was achieved with the application of the recovery device, and the total loss rate of the header reduced by 52.26%, which is of great significance in reducing the total loss rate of the combine harvesters and improving the operation performance of machinery. The research results can provide a reference for the design of the header structure of a rape combine harvester.

Keywords: rapeseed, combine harvester, side-cutting loss, coupled simulation, pneumatic recovery
DOI: 10.25165/j.ijabe.20221502.6267

Citation: Jiang T, Zhang M, Guan Z H, Mu S L, Wu C Y, Wang G, et al. Simulation and analysis of the pneumatic recovery for side-cutting loss of combine harvesters with CFD-DEM coupling approach. Int J Agric & Biol Eng, 2022; 15(2): 117–126.

1 Introduction

Rapeseed is a major oil crop and source of high-quality edible oil in China, with a regular cultivation area of approximately 6.6 million hectares. The rapeseed cultivated in China is a tall plant with dense, intertwining branches in the harvest season. A rapeseed header needs to be equipped with a vertical side-cutter on one side to cut these intertwining branches[1]. Mature rapeseed pods split easily. Under the shearing and vibration forces of the side-cutter, the pod splits, and the rapeseed scatters out of the header, resulting in high rapeseed losses[2-5]. Side-cutting loss accounts for approximately 40% of the total header loss[6], and header loss accounts for approximately 50% of the total combine harvester loss[7,8]. High harvester loss has been a critical factor limiting the development and improvement of mechanized combine harvesting of rapeseed[9].

Received date: 2021-08-25 **Accepted date:** 2022-03-08
Biographies: Tao Jiang, Assistant Researcher, research interests: agricultural mechanization engineering, Email: niam_justod@163.com; **Min Zhang**, Researcher, research interests: planting and harvesting machinery Email: Zhangmin01@caas.cn; **Senlin Mu**, Associate Researcher, research interests: agricultural mechanization engineering. Email: 398764546@qq.com; **Chongyou Wu**, Researcher, research interests: planting and harvesting machinery. Email: 542681935@qq.com; **Gang Wang**, Assistant Researcher, research interests: agricultural mechanization engineering. Email: 421404047@qq.com; **Haitong Li**, Assistant Researcher, research interests: agricultural intelligent equipment. Email: 764430096@qq.com.

***Corresponding author: Zhuohuai Guan**, Assistant Researcher, research interests: design and intelligent technology of combine harvester. Nanjing Institute of Agricultural Mechanization, Ministry of Agriculture and Rural Affairs, No.100 Liuying, Xuanwu District, Nanjing 210014, China. Tel: +86-25-84346229, Email: guan_zh@Foxmail.com.

In China, 85% of the cultivation area of rapeseed is located in the Yangtze River Valley[10-12]. In a paddy-upland rotation, rapeseed is usually grown in small paddocks with wet, soft soils and harvested by medium-to-small combine harvesters. These harvesters have narrow operating widths (below 2.5 m) and require many rounds of side-cutting operations, resulting in significant side-cutting loss[13,14]. In the US and Canada, rapeseed is grown in large areas of continuous paddocks and harvested by using large combine harvesters with ultra-wide operating width (above 9 m), which requires relatively less round of side cutting and thus incur the reduction of total less side-cutting loss. But the loss of one single round of side-cutting is not actually reduced and therefore a header with wide operating widths cannot fundamentally resolve the problem of high side-cutting loss.

Chinese researchers have investigated high header loss from the use of medium-to-small rapeseed combine harvesters. Chen[15] et al. attributed the large header rapeseed loss incurred by a grain combine harvester to pulling and impact forces exerted on the straw by the header and snapping roll. Therefore, the addition of a vertical side cutter on the unharvested side and a modification of the snapping roll parameters was proposed. Luo et al.[16] designed four straw separation devices that were mounted on the header to reduce rapeseed harvester loss. However, header loss from straw-pod pulling and dragging remained high. Ran et al.[17] designed a planet gear driver of the reciprocating double-acting cutter to solve the serious vibration, high rapeseed loss rate caused by the single-acting reciprocating cutter of the traditional rapeseed combine harvester. Li et al.[18] designed a disk cutter with an eccentric arc-shaped, toothed blade to reduce header loss, particularly for harvesting rapeseed. The inertial force of the cutter could easily be balanced to produce only small vibrations.

In addition, the sliding-cutting angle of the eccentric-arc-shaped blade increased gradually in the outward direction, reducing the cutting force on the straw and the drag and power consumption of the toothed blade and thereby, header loss. Wu et al.[19] conducted a series of bench tests to investigate the factors influencing the cutting force on oilseed rape straw, i.e., the cutting technique, the cutting position, the cutting blade geometry, and the cutting velocity. An optimal set of operating parameters for minimizing cutter loss was obtained. In the abovementioned studies, rapeseed header loss was reduced through technological means, such as adding accessory mechanisms, optimizing the header structure and operating parameters, and reducing cutter vibration and impact. However, side-cutter loss is caused by the impact and pulling forces exerted by the vertical cutter on the rapeseed pod and cannot be completely eliminated by improvements in the mechanical structure or optimization of the operating parameters. Some researchers have studied pneumatic devices to reduce the header loss[20-23], but rarely focused on recovering the side-cutting loss. Reducing the side-cutting loss of rapeseed headers remains an urgent technological challenge, and few studies were reported on this topic.

To address the abovementioned problems, a novel pneumatic recovery method was proposed and a device using sweeping-and suction airflows was designed in this study to recover side-cutting loss for rapeseed combine harvesters. The performance and operating parameters of the pneumatic recovery device were analyzed and optimized by using CFD-DEM coupled simulation. The effects of the airflows on the motion of rapeseed particles and impurities in the device were investigated. The simulation results were compared with the results of a series of field tests performed on the device. Acceptable device performance for recovering rapeseed side-cutting loss was found in this parametric setting. The study can provide input for the structural design of rapeseed headers.

2 Materials and methods

2.1 Collection and composition determination of the scattered materials

Cutting and pulling forces exerted by the vertical side cutter on rapeseed lead to both seeds and materials rather than seeds. A field test was conducted to analyze the components of the collected mixture to improve the accuracy of the parametric settings for subsequent simulation.

The test was carried out in Minle County, Zhangye in Gansu province on September 21, 2019. The rapeseed cultivar was Kele 521, with 3.5 g per 1000 seeds. In order to collect the scattered materials caused by side-cutting, a sampling tank was hung at the bottom of the vertical cutter, as shown in Figure 1. The material in the tank was collected after each test.

Figure 1 Overall structure of the collection tank

Three groups with a stroke of 10 m were set in the test. The combine harvester operated at a preset period of time, and each group was repeated thrice. The collected materials were classified and counted, and the results showed that seeds, silique pods, and short stems were included in the scattered materials, as shown in Figure 2.

Figure 2 Scattered materials

According to the statistical results, the production rates of seeds and impurities were calculated at each machine speed, as listed in Table 1. The number of rapeseeds and impurities were the total quantities of scattered materials that fell into the collection tank in each test. The impurity-seed ratio was the ratio of their quantities, which would be used in the following simulation. Also the generation rate would decide some parameter settings in the simulation.

Table 1 Determination test results

No.	Advance speed /m s^{-1}	Number of rapeseeds	Generation rate of rapeseed piece/s	Number of impurities	Generation rate of rapeseed piece/s	Impurity-rapeseed ratio
1	0.8	2900	232	638	51	0.22
2	1	4320	432	1250	125	0.29
3	1.2	6150	723	2460	290	0.45

2.2 Methods of recovering side-cutting loss

As mentioned above, the side-cutting loss cannot be totally avoided by changing the header structure or operation parameters of the combine harvester. Therefore, it is recommended that a recovery device could be constructed to collect the scattered materials and convey them to the header during operation of the combine harvester, thus reducing side-cutting loss.

According to this proposed method and in combination with the advantages of pneumatic conveying, the prototype of the pneumatic recovery device was constructed, considering the structural constraints of the vertical cutter, as shown in Figure 3. During the combine harvester operation, the scattered materials fall into the collection area, and the airflow with high velocity generated by the fan has an effect on the materials in the area, pushing them into the conveying pipeline, and then returning to the header to complete the recovery.

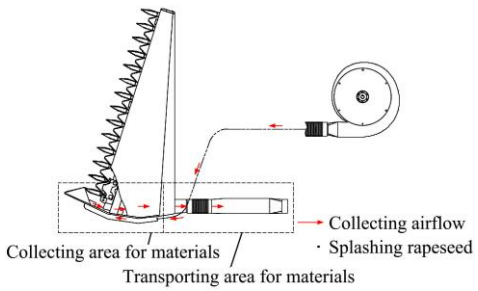

Figure 3 Sketch of airflows and the material transportation path

2.3 Simulation model and parameters

2.3.1 Mathematical model of gas-solid flow

The volume fraction of solid particles is less than 10% for the gas-solid two-phase flow involved in the rapeseed loss recovery operation. The Eulerian model can be solved using a multiphase flow framework including a volume fraction term to consider the effect of particles on the flow field[24]. An Eulerian-Lagrangian coupled model was used for the simulation analysis. The continuity equation, the Navier-Stokes equation, and the standard *k-ε* turbulence model were solved within the Eulerian coordinate system to determine the gas flow field in the device. The equations of motion for the particles were solved within the Lagrangian coordinate system[25]. The coupling between the gas and solid flows was computed by iteratively computing the drag force on the particles and the momentum exchange between the particles.

The continuity equation of fluid phase can be expressed as

$$\frac{\partial \varepsilon \rho}{\partial t} + \nabla \rho \varepsilon u = 0 \tag{1}$$

where, ρ is density of airflow, kg/m^3; t is the time, s; u is airflow velocity, m/s; ε is volume fraction.

The momentum conservation could be expressed as

$$\frac{\partial \varepsilon \rho u}{\partial t} + \nabla(\rho \varepsilon u^2) = -\nabla \rho + \nabla(\mu \varepsilon \nabla u) + \rho \varepsilon g - S \tag{2}$$

$$S = \frac{\sum_{i=1}^{n} F_{D,i}}{V} \tag{3}$$

where, g is gravity; μ is dynamics viscosity coefficient; S is the momentum exchange between solid and gas phases due to forces exerted by airflow on all particles within the computational cell; $F_{D,i}$ is fluid resistance; V is cell volume in CFD; ∇ is the Hamiltonian differential operator

The drag force constitutes the dominant effect of the airflows on the rapeseed grain, whereas the Saffman lift force and the Basset force are negligible. Therefore, a free-stream drag force model was used[26-28]. The force on the particles was calculated from the following equations,

$$F_{D,i} = 0.5 C_D \rho A |u - u_p| (u - u_p) \tag{4}$$

where, C_D is the drag coefficient calculated as given by Sommerfeld[29]; A is projected area of solid term, u_p is velocity of solid term.

The C_D was determined by the Reynolds number R_e

$$C_D = \begin{cases} \dfrac{24}{Re} & (Re \le 0.5) \\ \dfrac{24(1 + 0.25 Re^{0.687})}{Re} & (0.5 < Re \le 1000) \\ 0.44 & (Re > 1000) \end{cases} \tag{5}$$

$$Re = \frac{\rho L |u - u_p|}{\mu} \tag{6}$$

where, d is particle diameter, m.

2.3.2 DEM contact model

Within the DEM, which is based on the Lagrangian method, a large number of discrete particles is simplified into an aggregate of particles with a specific geometry and mass, and contact-mechanics models with predefined parameters are used to simulate the contact between particles, as well as between particles and the boundary. That is, DEM considers the effects of contacts between particles and between particles and the boundary and the physical-mechanical properties of the particles and the boundary. Contact can be simulated using two different models: rigid-spherical and soft-spherical. Within the soft-spherical contact model, inner particle contacts are allowed to overlap, and the contact force is computed based on the mechanical properties, the magnitude of normal overlap, and the tangential displacement of inner particle contact. Considering the absence of adhesion between rapeseed particles[30], the Herts-Mindlin nonslip soft-spherical contact model was used for the simulation analysis.

2.3.3 Models and parametric settings

A three-dimensional model of the recovery device was gridded using ANSYS Workbench, as shown in Figure 4.

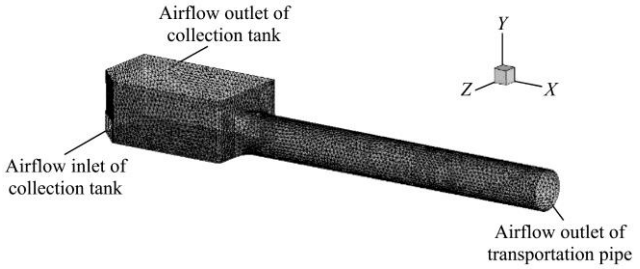

Figure 4 Schematics of computational grids

Considering that the rapeseeds and pods constituted more than 94%w.t. of the materials in the collection tank, the simulation was simplified by simulating only rapeseeds and silique pods (impurities) and neglecting other impurities.

The impurity to rapeseed ratio in Table 1 was used for the Particle Factory in EDEM (Engineering discrete element method) software as 0.22:1. Relevant parameters of the rapeseed and impurities from the literature[31] were used to establish the particle models, as shown in Figure 5.

a. Rapeseed b. Impurity

Figure 5 DEM models of materials

Eulerian-Lagrangian coupling was used in the DEM-CFD coupled simulation. A theoretical analysis showed that airflows exerted the following forces on the particles: the freestream-equation fluid drag, the Saffman lift, and the Magnus lift. The airflows were defined as turbulences. The standard *k-ε* turbulence model and the standard wall functions in Fluent software were used to simulate the continuous-phase airflow field. The pressure-velocity scheme was set as SIMPLEC. The spatial discretization was set in second order.

The housing of the recovery device prototype was made from steel plate. Table 2 lists the mechanical properties of the particles, the steel plate, and the contact between the materials[32]. The total number of generated rapeseed and impurities were 1000 and 220. The time steps of the EDEM and CFD simulations were 3×10^{-5} and 1.5×10^{-3} s, respectively. The simulations were run for a total of 5 s.

3 Simulation results and analysis

The effects of different recovery methods were analyzed by clarifying the movement rules of materials under the effect of different airflow fields. And the most suitable pneumatic recovery method and the optimal parameters were obtained by a series of simulations.

Table 2 Mechanical properties

Category	Parameter	Value
Rapeseed	Axes/mm×mm×mm	2×2×2
	Poisson's Ratio	0.25
Impurity	Diameter/mm	4
	Length/mm	45-65
	Poisson's Ratio	0.4
Rapeseed-impurity	Coefficient of restitution	0.3
	Coefficient of static friction	0.4
	Coefficient of rolling friction	0.01
Rapeseed-rapeseed	Coefficient of restitution	0.6
	Coefficient of static friction	0.5
	Coefficient of rolling friction	0.01
Rapeseed-device	Coefficient of restitution	0.6
	Coefficient of static friction	0.3
	Coefficient of rolling friction	0.01
Impurity-impurity	Coefficient of restitution	0.2
	Coefficient of static friction	0.4
	Coefficient of rolling friction	0.01
Impurity-device	Coefficient of restitution	0.2
	Coefficient of static friction	0.5
	Coefficient of rolling friction	0.01

In this section, the evaluation index of the recovery effect was defined as recovery rate. It was counted in the EDEM software post processing part and calculated by the percentage of the total number of rapeseeds passed through the transportation pipe to the total number of rapeseeds generated, so as to determine the best pneumatic recovery method and operation parameters of the device and improve the recovery rate of scattered seeds.

3.1 Analysis of different pneumatic recovery methods on recovery rate

3.1.1 Analysis of air-sweeping recovery method on recovery rate

As shown in Figure 3, the sweeping airflow generated by the fan entered the collection tank through the inlet. The airflow affected the materials in the tank and made them move towards the transportation pipe.

The air-sweeping recovery method was applied with a 15 m/s airflow velocity at the collection tank inlet, and the recovery performance was simulated. Figure 6 showed the airflow velocity contour in the *X*-direction at Plane $Y = -15$ mm. Figure 7 showed the motion of particles under the effect of the airflow.

Figures 6 and 7 showed that the airflow transported the materials at the front of the collection tank to the transportation pipe inlet. However, the airflow in the pipe had a low *X*-velocity and exerted insufficient force on the materials. Thus, the majority of the materials were heaped in the pipe, and only a small proportion of the seeds were transported through the pipe, resulting in a low seeds recovery rate. The velocity of the airflow at the collection tank inlet was increased to improve particle transport by the airflow. Figure 8 showed the seeds recovery rates for different velocities of the air-sweeping airflow.

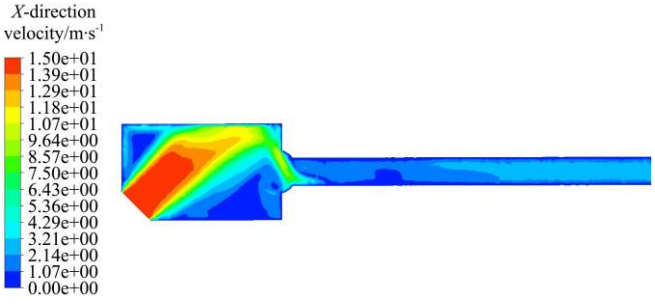

Figure 6 *X*-direction velocity contour of air-sweeping flow field

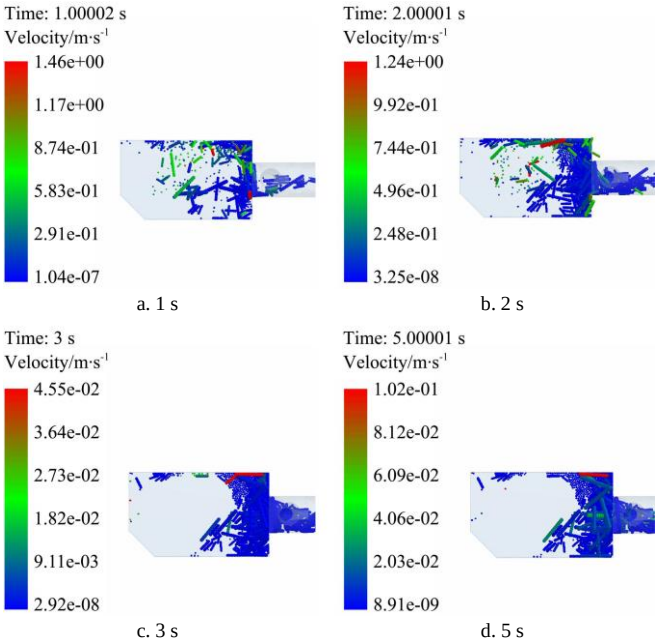

Figure 7 Materials motion in air-sweeping flow field

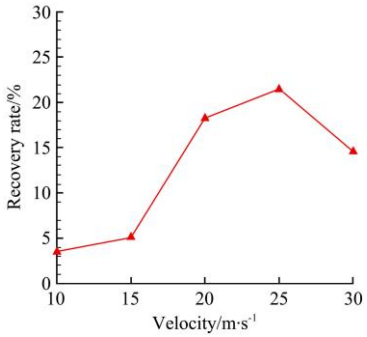

Figure 8 Relationship between sweeping airflow velocity and recovery rate

Figure 7 showed that the seeds recovery rate increased slightly with the velocity but did not attain an acceptable value. Increasing the airflow velocity to above 25 m/s resulted in disordered particle motion in the collection tank and decreased the recovery rate.

The simulation showed that the airflow was reflected at the wall and arrived at the inlet of the transportation pipe with a markedly decreased *X*-velocity. The airflow exerted a smaller force on the materials than the friction between them. The seeds barely entered the long and narrow transportation pipe from the collection area, resulting in heaps along the transportation path. Therefore, a desirable recovery rate cannot be achieved by applying the air-sweeping method alone.

3.1.2 Analysis of air-suction recovery method on recovery rate

The recovery device was improved and a suction airflow generator was added[33], the three-dimensional model was gridded as shown in Figure 9.

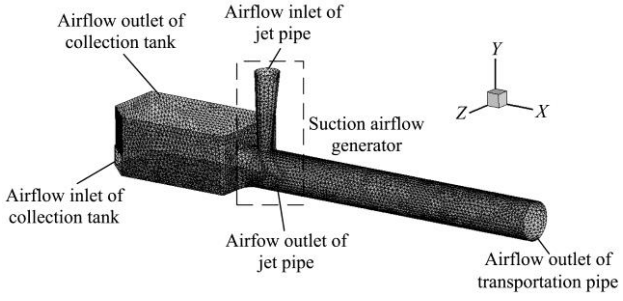

Figure 9 Improved recovery device

The suction airflow generator is based on Bernoulli's principle. Figure 10 showed the structure of the generator.

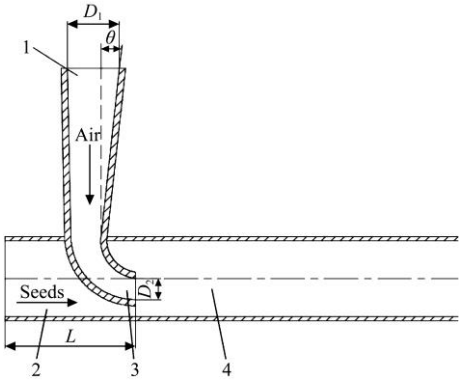

1. Airflow inlet of the jet pipe 2. Inlet of the transportation pipe 3. Airflow outlet of the jet pipe 4. Mixture chamber

Figure 10 Structure of the generator

The recovery device performance was simulated under the application of a single air-suction recovery method. The airflow velocity at the jet pipe inlet was set at 15 m/s. Figure 11 showed the airflow velocity contour in the *X*-direction at Plane $Y = -15$ mm of the recovery device. Figure 12 showed the motion of materials under the effect of the airflow.

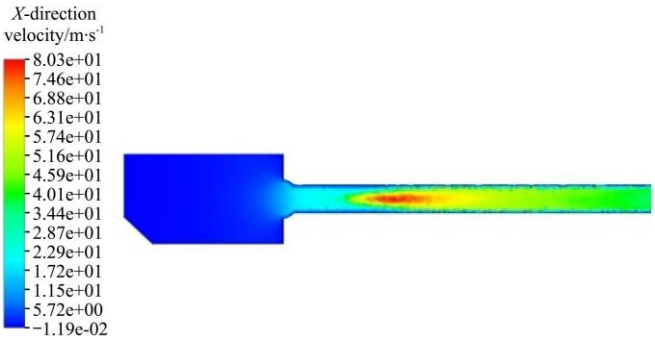

Figure 11 X–direction velocity contour of air–suction flow field

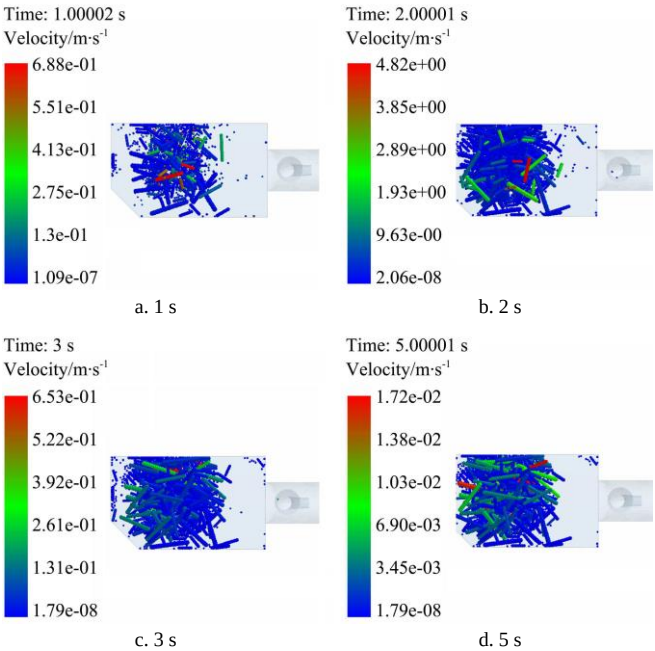

Figure 12 Materials motion in air–suction flow field

Figure 11 shows that compared with the simulation results for applying only the air-sweeping method, the airflow velocity at the inlet of the transportation pipe increased markedly, thus improving the suction and transportation of materials in these areas. Figure 12 shows that the materials in the vicinity of the transportation pipe inlet were smoothly sucked in, however, the airflow velocity in the open area away from the transportation pipe decreased markedly along the negative *X*-axis. The airflow only moved materials over a small area, and the suction was not sufficiently strong to move materials far from the transportation pipe, resulting in heaps at the front of the collection tank.

In the following simulation, the jet-pipe inlet velocity was increased to a higher level, so as to enhance the suction capacity. However, with the increasing of the jet-pipe inlet airflow velocities, materials still formed heaps at the front of the collection tank at the end time (5 s) of each simulation, indicating that suction by the airflow did not increase with the airflow velocity, as shown in Figure 13. Therefore, a desirable recovery rate cannot be achieved by applying air–suction recovery method alone.

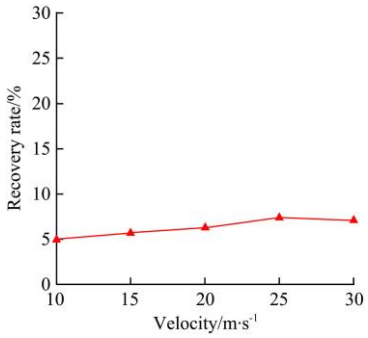

Figure 13 Relationship between suction airflow velocity and recovery rate

3.1.3 Analysis of composite pneumatic recovery method on recovery rate

The recovery device performance was simulated under both air-sweeping and air-suction methods. Figure 14 shows the airflow velocity contour in the *X*-direction at Plane $Y = -15$ mm of the recovery device, for airflow velocities at the inlets of 15 m/s. Figure 15 shows the motion of materials under the effect of the airflows.

Figures 14 and 15 show that the propulsion and directing effects of the sweeping airflow transported particles to the area where the airflows converged. Upon being transported to the area covered by the suction airflow, materials were sucked into the pipe and transported further down the transportation path, thereby realizing rapeseeds recovery.

3.1.4 Discussion of the different pneumatic recovery methods

Figure 16 shows the air velocity curves along the *X*-direction of each flow field at Plane $Y = -15$ mm of the recovery device in different pneumatic methods.

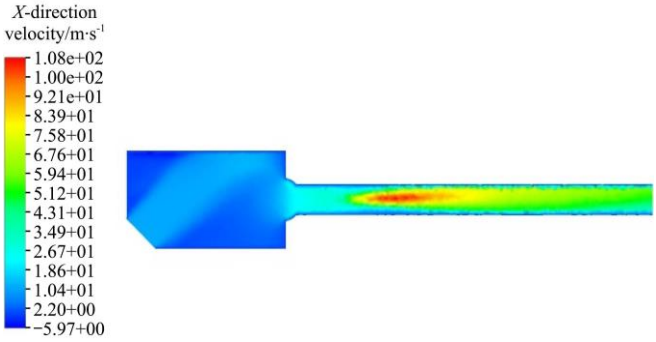

Figure 14 *X*-direction velocity contour of composite pneumatic flow field

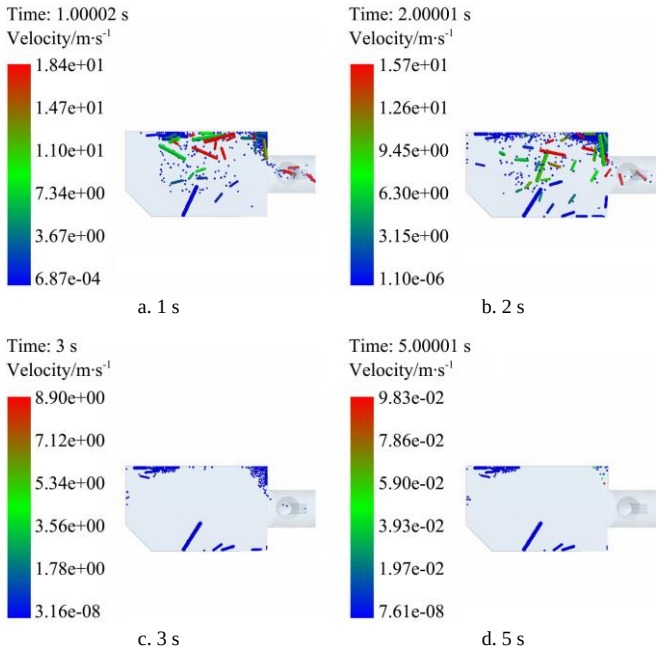

Figure 15 Materials motion in composite pneumatic flow field

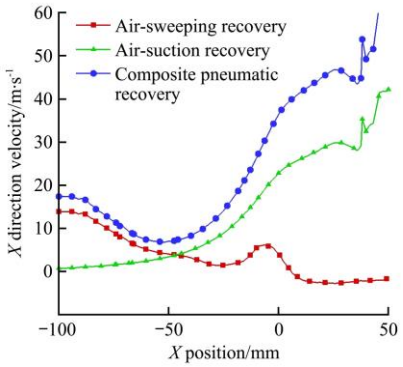

Figure 16 Comparison of *X*-direction velocity of different pneumatic method

Figure 16 depicted that in the entrance area of the conveying pipe ($X = -10$ mm), the flow field velocity in the air suction and composite recovery method was relatively high. The materials can be conveyed to the pipe under the action of the airflow and were rapidly recovered under the push of the high-speed airflow in the pipeline. However, the airflow velocity of the flow field in the air-sweeping recovery method was significantly attenuated in this area. As a result, the thrust on the materials was insufficient and the materials accumulated as they were difficult to enter the conveying pipe. Although the air suction recovery method had a significant effect on the entrance area of the conveying pipe and the materials inside the pipe, the air velocity at the front end (-100 mm $\leq X \leq -50$ mm) of the device was greatly attenuated, which could not meet the movement requirements of the materials.

The analysis above showed that the side-cutting loss during the combine harvesting operation could not be effectively recovered via the sweeping effect of a positive-pressure airflow alone or the suction effect of a negative-pressure airflow alone. However, the loss could be effectively recovered by combining sweeping-suction airflows, thereby simultaneously exerting collecting, suction, directing, and transporting effects on materials.

3.2 Analysis of impact of material status on recovery rate

From the statistical test results in Section 2.1, it can be seen that the status of the scattered materials was not constant, including the composition ratio and the quantity of materials, namely, the rate of material generation. Therefore, after the determination of the overall recovery method, it was also necessary to clarify the influence of the material status on the seed recovery performance.

3.2.1 Analysis of material composition ratio on recovery rate

A series of single-factor tests were conducted based on the obtained impurity-to-seed ratio (Section 2.1). Composite pneumatic recovery method was applied with a 15 m/s airflow velocity at both the collection tank inlet and the jet pipe inlet. The airflow field model and airflow parameters were not changed. The total quantity of seeds was set as 500 and the impurity-to-seed ratio varied from 0.1 to 0.5 as the interval was 0.1. The simulation was simplified by setting the mean impurity length at 45 mm. The simulation was run several times, and the rapeseed recovery rate was recorded for each run.

Figure 17 demonstrated that at impurity-to-rapeseed ratio below 0.3, the quantity of impurities did not have a significant influence on the high rapeseed recovery rate. As the impurity-to-rapeseed ratio increased, the rapeseed recovery rate decreased gradually. This result may be explained by the following mechanism observed during the simulation. An increase in the quantity of impurities reduced the effect of the airflows on the rapeseed and increased the probability of blockage of the transportation pipe inlet, thereby impeding the rapeseed transportation and reducing the recovery rate.

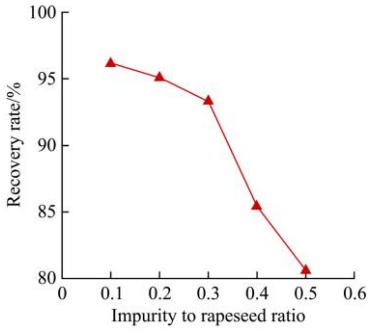

Figure 17 Influence of impurity to rapeseed ratio on recovery rate

3.2.2 Analysis of materials generation rate on recovery rate

A combine harvester advances at varying velocities during operation, thus, the rate of side-cutting loss varies, along with the quantity of scattered materials per unit time. The effects of these variations on the loss recovery rate were determined by varying the particle generation rates in the EDEM Particle Factory, thereby simulating the varying loss rates caused by different combine harvester advance speeds. The total quantities of impurities and rapeseed were not controlled. The airflow velocities at the inlets were set at 15 m/s. All other parameters remained unchanged. The generation rates of seed and impurity used in the simulation were set based on the test results shown in Table 1 of Section 2.1. According to the test results, the generation rate and the corresponding advance speed of the machine are listed in Table 3.

Table 3 Generation rate of materials

No.	Generation rate/piece s^{-1}		Corresponding advance speed of the machine/m s^{-1}
	Seed	Impurity	
1	250	50	0.8
2	430	125	1
3	700	290	1.2

Table 4 lists the recovery rate per second obtained from the simulation runs.

Figure 18 shows the simulated recovery rates for different generation rates. For all the simulation runs, a low recovery rate

was obtained in the first second because of the finite time for the rapeseed to fall into the collection area, that is, there is a time lag between rapeseed recovery and collection. During the simulation run for test No.1, the recovery rate gradually increased and then stabilized at a high level as the duration of simulation increased. As the feed rates or the quantity of impurities generated in a unit time were increased, it became more difficult for the rapeseed to enter the transportation pipe. Thus, the quantity of heaped materials gradually increased, and the recovery rate gradually decreased. During the simulation run for test No.3, the quantity of impurities heaped at the inlet of the transportation pipe increased as the duration of simulation increased. Thus, seeds were prevented from entering the transportation pipe, and the recovery rate decreased markedly. Therefore, the airflow velocities at the inlets set for the simulation could not achieve a desirable recovery rate at this feed rate.

Table 4 Simulation results

No.	Simulation Time/s	Recovery rate/%
1	1	69.6
	2	85.8
	3	95.2
	4	97.6
	5	96.4
2	1	65.4
	2	82.3
	3	88.2
	4	76.2
	5	73.1
3	1	41.4
	2	60.4
	3	52.5
	4	22.6
	5	17.3

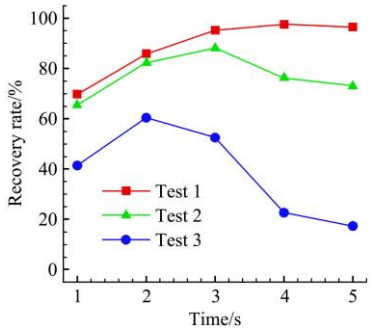

Figure 18 Relationship between recovery rate and time

It can be concluded from the simulation results that under the action of the composite pneumatic recovery method, as the impurity-to-rapeseed ratio was above 0.3 and the material generation rate corresponded to the forward speed of the harvester above 1 m/s, the flow field parameters settings could no longer meet the requirements of seed recovery, indicating when the material status exceeded this critical condition, the recovery decreased. It was necessary to adjust the operation parameters to improve the adaptability of the recovery device.

3.3 Parameter optimization of inlets velocity

Combined with Section 3.1 and Section 3.2, the operation parameters of the composite recovery should be adjusted under the critical condition, as they were no longer suitable for a desirable recovery rate, and the simulation of airflow velocity optimization was carried out.

The effects of the sweeping and suction airflow velocities on the recovery rate were analyzed by a series of simulations. The simulations were run at the following parametric settings: impurity-to-rapeseed ratio: 0.4; rapeseed generation rate: 550 pieces/s; total quantity of rapeseed: 2750 pieces; impurity generation rate: 200 pieces per second: total quantity of impurities: 1000 pieces; The other simulation parameters remained unchanged. Table 5 showed the settings and results of the simulations.

Table 5 Simulation results of recovery rate

No.	X_1 Airflow velocity of collection tank inlet/m s^{-1}	X_2 Airflow velocity of jet pipe inlet/m s^{-1}	Recovery rate/%
1	15	15	85.1
2	15	20	89.2
3	15	25	92
4	20	15	92.6
5	20	20	94.7
6	20	25	97.2
7	25	15	91.8
8	25	20	93.2
9	25	25	93.9

Table 6 lists the results of a variance analysis that was performed on the simulation results.

Table 6 Variance analysis of inlet velocities

Source	SS	df	MS	*F*	*p*-value	*F* crit
X_1	166.04	2	83.02	99.09	1.92E-10	3.55
X_2	87.1	2	43.55	51.98	3.32E-08	3.55
Interaction	18.08	4	4.52	5.39	0.0049	2.93
Total	286.29	26				

Table 6 lists that the airflow velocities at both the inlets of the collection tank and the jet pipe considerably affected the recovery rate, where the former had a more significant influence than the latter.

Figure 19 showed a three-dimensional representation of the correlation between the recovery rate and the airflow velocities at the inlets of the collection tank and the jet pipe.

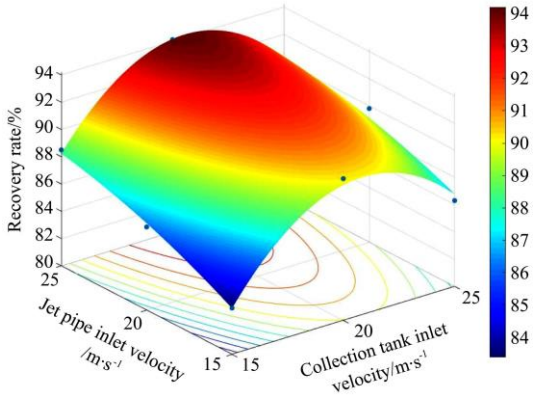

Figure 19 Correlation between the recovery rate and the airflow velocities

Figure 19 shows that at all the different airflow velocities at the jet pipe inlet, the recovery rate first increased and then decreased slightly as the airflow velocity at the collection tank inlet increased. This result can be explained by the following mechanism. As the airflow velocity at the collection tank inlet increased, the airflow had an excessive effect on the falling materials, resulting in disordered particle motion in the collection tank. Increased collisions between materials and the wall made it more difficult for the seeds to enter the transportation pipe. At all the different

airflow velocities at the collection tank inlet, the recovery rate increased with the airflow velocity at the generator inlet. Thus, a high suction airflow velocity significantly affected the particles in the vicinity of the transportation pipe inlet, thereby reducing the quantities of impurities and rapeseed particles stagnating and heaping in this area and facilitating smoother rapeseed transportation. The simulation results showed that acceptable performance of the rapeseed recovery device was obtained under normal operation of the combine harvester. More specifically, the device can achieve an average rapeseed recovery rate of 96.7% for airflow velocities of 20 m/s and 25 m/s at the inlets of the collection tank and the generator, respectively.

4 Field test

4.1 Test conditions

Based on the prior research conclusions, a composite pneumatic recovery device was constructed and installed on the combine harvester header, as shown in Figure 20.

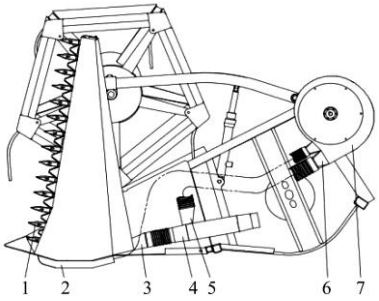

1. Side cutter 2. Airflow inlet of the collection tank 3. Collection tank 4. Transportation pipe 5. Suction airflow generator 6. Airflow distributor 7. Fan

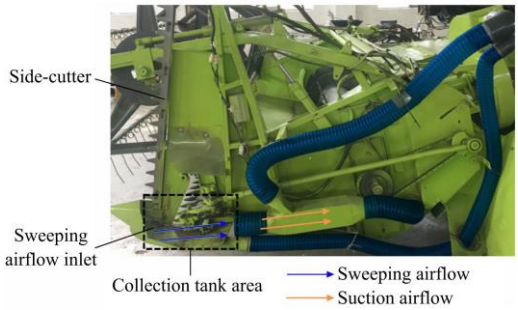

Figure 20 Inner structure of the collection tank

In order to verify the operation effect of the composite pneumatic recovery device, a field test was conducted in Dafeng District, Yancheng, Jiangsu province in June 2020. The rapeseed cultivar was Kele 521, with 3.5 g/1000 seeds, 18% moisture content, and a theoretical seed harvest quality of 450 g per square meter. The advance speed of the harvester was fixed at 1.2 m/s.

Due to the convenient adjustment for different revolving speed, a hydraulic driven fan was used to generate the required airflow for the field test. And an anemograph was used to measure the airflow velocity of different airflow inlets to ensure the consistency of velocity parameters between the simulation and field tests, as shown in Figure 21.

Due to the control precision of the revolving speed of the fan, the parameters used in the validation tests were controlled to approximately match the analytically optimized values obtained by the simulation in Section 3.2.3, as the collection tank inlet airflow velocities of 20 m/s and the generator inlet airflow velocities of 25 m/s. All other structures and operation parameters remained the same. The picture of the test site is shown in Figure 22.

Figure 21 Airflow velocity measurement

Figure 22 Field test

Four test areas were randomly selected in the field to conduct a series of tests, and a 20 m long testing zone was selected in each test area, and five sampling points were randomly selected in the testing zone to sample and calculate the recovery rate of scattered seeds and the total loss reduction ratio of the header. The calculation formula is shown as follows:

$$Y_1 = \frac{W_3}{W_2 + W_3} \times 100\% \quad (7)$$

$$Y_2 = \frac{W_3}{W_1 + W_2 + W_3} \times 100\% \quad (8)$$

where, Y_1 is the recovery rate of side-cutting loss, %; Y_2 is the header loss reduction ratio, %; W_1 is the mass of the seed loss excluding side-cutting, g; W_2 is the mass of the seeds left in the collection tank of the recovery device, g; W_3 is the mass of the recovery seed, g.

W_1 was measured by the sampling box which was put in the operation route of combine harvester. After each test, the materials in the box were accounted and thus the mass of the seed loss excluding side-cutting of the header could be calculated proportionately.

4.2 Field test results and discussion

The results of the field tests are listed in Table 7. The average recovery rate was 92.95%, which differed from the results obtained from the simulation of section 3.2.3 by 3.9%. Even though there was an absolute numerical error in the final recovery rate, the rationality of the simulations was verified. Discrete particles exhibit completely random motion, there are inconsistent collisions between rapeseed and other particles, and the particles have inconsistent morphologies. And due to the inconsistent cropping intensity, the quantity of scattered materials that fell into the collection tank changed during the operation, which affected the recovery rate, too. Therefore, difference existed between the recovery rates obtained from the field test and the simulation results.

The total loss rate of the combine harvester header reduced by 52.26% after the recovery device installed, which indicated that the pneumatic recovery method and device can effectively reduce the loss rate of the side-cutting loss in the rapeseed combine harvesting.

Table 7 Field test results

No.	W_1/g	W_2/g	W_3/g	Y_1/%	Y_2/%
1	310	20	345	94.52	51.11
2	281	31	366	92.19	53.98
3	346	42	403	90.56	50.95
4	298	35	391	91.78	54.01
Average				92.95	52.26

The results of the field tests also reflected that some improvement needed to be made in the material discrete models building and parameters setting, this would be the most important part of work in the future research.

5 Conclusions

In this study, the CFD-DEM coupled method was used to simulate the pneumatic recovery of the side-cutting loss in the rapeseed combine harvesting, and field verification tests were conducted and the following conclusions were drawn.

(1) The composition of the scattered side-cutting loss was determined through field tests. The impurity-seed ratio and the generation rate at different harvester advance speed were measured and calculated.

(2) An optimal recovery method and operating parameters to reduce the side-cutting loss was determined by using a series of simulations. And the specific critical condition under which the congestion occurred was investigated.

(3) The average rapeseed recovery rate of 92.95% was achieved from a series of field tests, and the total loss rate of the header reduced by 52.26%. It is of great significance to improve the operation quality of the combine harvester.

Acknowledgements

This work was supported by the Key Research Program & Technology Innovation Program of Chinese Academy of Agricultural Sciences (CAAS-ZDRW202105); China Agriculture Research System of MOF and MARA (CARS-12); Synergistic Innovation Center of Jiangsu Modern Agricultural Equipment and Technology (4091600002); Central Public-interest Scientific Institution Basal Research Fund for Chinese Academy of Tropical Agricultural Sciences (S202102-02).

[References]

[1] Xu L Z., Li Y M, Ma C X, He Z F, Lv F. Design of main working parts of 4LYB1-2.0 rape combine harvester. Transactions of the CSAM, 2008; 39(8): 54–57, 58. (in Chinese)

[2] Hobson R N, Bruce D M. Seed loss when cutting a standing crop of oilseed rape with two types of combine harvester header. Biosystems Engineering, 2002; 81(3): 281–286.

[3] Bruce D M, Farrent J W, Morgan C L. Determining the oil rape pod strength needed to reduce seed loss due to podshatter. Biosystems Engineering, 2002; 81(2): 179–184.

[4] Szpryngiel M, Wesołowski M, Szot B. Economical technology of rape seed harvest. Teka Komisji Motoryzacji IEnergetyki Rolnictwa, 2003; 4(1): 185–195.

[5] Wang R, Ripley V L, Rakow G. Pod shatter resistance evaluation in cultivars and breeding lines of *Brassica napus*, *B. juncea* and *Sinapis alba*. Plant Breeding, 2010; 126(6): 588–595.

[6] Ma N, Zhang C L, Li J, Zhang M H, Cheng Y G, Li G M, Zhang S J. Mechanical harvesting effects on seed yield loss, quality traits and profitability of winter oilseed rape (*Brassicanapus* L.). Journal of Integrative Agriculture, 2012; 11(8): 1297–1304.

[7] Li H T, Li Q X, Li P, Huang P, Wang X Y, Ji M Y. Design on separating-combined header of rape combine harvester. Journal of Huazhong Agricultural University, 2014; 5: 111–116. (in Chinese)

[8] Chai X Y, Xu L Z, Yan C, Liang Z W, Ma Z, LI Y M. Design and test of cutting frequency follow-up adjusting device for vertical cutting knife of rapeseed cutting machine. Transactions of the CSAM, 2018; 49(12): 93–99. (in Chinese)

[9] Huang X M, Zong W Y. Research status and development trend of rape combine harvester. Agricultural Engineering, 2012; 2(1): 14–19. (in Chinese)

[10] Wang H Z. New-demand oriented oilseed rape industry developing strategy. Chinese Journal of Oil Crop Sciences, 2018; 40(5): 613–617. (in Chinese)

[11] Zhang Q S, Zhang K, Liao Q X, Liao Y T, Wang L, Shu C X. Design and experiment of rapeseed aerial seeding device used for UAV. Transactions of the CSAE, 2020; 36(14): 138–147. (in Chinese)

[12] Lyu W S, Xiao X J, Xiao G B, Huang T B, Xiao F L, Li Y Z, et al. Effects of lateral deep application and dosage of slow-release fertilizer on yield and fertilizer utilization efficiency of rape (*Brassica napus* L.). Transactions of the CSAE, 2020; 36(19): 19-29. (in Chinese)

[13] Wu C Y, Xiao S Y, Jin M. Comparation on rape combine harvesting and two-stage harvesting. Transactions of the CSAE, 2014; 30(17): 10–16. (in Chinese)

[14] Guan Z H, Wu C Y, Wang G, Li H T, Mu S L. Design of bidirectional electric driven side vertical cutter for rape combine harvester. Transactions of the CSAE, 2019; 35(3): 1–8. (in Chinese)

[15] Chen C Y, Wang X Z, He Z F. Design of header for rape harvesting using grain combine harvester. Transactions of the CSAM, 2003; 34(5): 54–56, 60. (in Chinese)

[16] Luo H F, Tang C Z, Guan C Y, Wu M L, Xie P F. Experiment using stalk separator designed for the header of rape harvester. Journal of Hunan Agricultural University, 2012; 38(5): 548–550. (in Chinese)

[17] Ran J H, Mu S L, Li H T, Guan Z H, Tang Q, Wu C Y. Design and test of planet gear driver of reciprocating double-acting cutter for rapeseed combine harvester. Transactions of the CSAE, 2020; 36(9): 17–25. (in Chinese)

[18] Li Z K, Xie P F, Liu K, Tang X, Wang X S, Mao L C. Design and performance evaluation of a disc cutter for rape harvest. Journal of Hunan Agricultural University, 2014; 40(1): 83–88. (in Chinese)

[19] Wu M L, Guan C Y, Tang C D, Chen S Y, Luo H F, Xie P F. Experiments on influencing factors of cutting force of rape stem. Transactions of the CSAE, 2009; 25(6): 141–144. (in Chinese)

[20] Li Y N, Yi Y W, Du S W, Ding Q S, Ding W M. Design and experiment on air blowing header of plot combine harvester for grain. Transactions of the CSAM, 2017; 48(6): 79–87. (in Chinese)

[21] Pan H B, Wang T T, Huang X M, Zha X T, Zong W Y. Numerical simulation of drifting process of oil rape seeds in a longitudinal positive pressure airflow field of the cutting platform. Journal of Huazhong Agricultural University, 2015; 34(3): 117–123. (in Chinese)

[22] Zong W Y, Huang X M, Pan H B, Zha X T, Wang T T. Drifting property of falling oil rape seeds in longitudinal positive pressure airflow field without stalks. Transactions of the CSAE, 2015; 31(3): 70–76. (in Chinese)

[23] Huang X M, Zha X T, Zong W Y, Chen H. Design and test of transverse positive pressure airflow collection device for header losses of rape combine harvester. Transactions of the CSAM, 2016; 47(S1): 227–233. (in Chinese)

[24] Chu K W. CFD-DEM simulation of the effect of particle density distribution on the multiphase flow and performance of dense medium cyclone. Minerals Engineering, 2009; 22(11): 893–909.

[25] Lei X L, Liao Y T, Zhang W Y. Li S S, Wang D, Liao Q X. Simulation and experiment of gas-solid flow in seed conveying tube for rapeseed and wheat. Transactions of the CSAM, 2017; 48(3): 57–68. (in Chinese)

[26] Liu L Y, Hao S Y, Zhang M, Liu D M, Jia F G, Quan L Z. Numerical simulation and experiment on paddy ventilation resistance based on CFD-DEM. Transactions of the CSAM, 2015; 46(8): 27–32, 158. (in Chinese)

[27] Jiang E C, Sun Z F, Pan Z Y, Wang L Y. Numerical simulation based on CFD-DEM and experiment of grain moving laws in inertia separation chamber. Transactions of the CSAM, 2014; 45(4): 117–122. (in Chinese)

[28] Khatchatourian O A, Toniazzo N A, Gortyshov Y F. Simulation of airflow in grain bulks under anisotropic conditions. Biosystems Engineering, 2009; 104(2): 205–215.

[29] Sommerfeld M. Analysis of collision effects for turbulent gas–particle flow in a horizontal channel: Part I. Particle transport. International Journal of Multiphase Flow, 2003; 29(4): 675–699.

[30] Boac J M, Casada, M E, Maghiang, R G. Material and interaction properties of selected grains and oilseeds for modeling discrete particles. Transactions of ASABE, 2010; 53(4): 1201–1216.

[31] Chen L, Liao Q X, Zong W Y, Liao Y T, Li H T, Huang P. Aerodynamic characteristics measurement of extraction components for rape combine harvester. Transactions of the CSAM, 2012; 43(S1): 125–130. (in Chinese)

[32] Lei X L, Liao Y T, Liao Q X. Simulation of seed motion in seed feeding device with DEM-CFD coupling approach for rapeseed and wheat. Computers and Electronics in Agriculture, 2016; 131: 29–39.

[33] Efrain Q P, Richart V R, Raul L A, Victor M B H. An approach to evaluate Venturi-device effects on gas wells production. Journal of Petroleum Science and Engineering, 2014; 116: 8–18.